Available online at www.sciencedirect.com

ScienceDirect

IFAC Papers Online CONFERENCE PAPER ARCHIVE

IFAC-PapersOnLine 49-18 (2016) 182–187

Resolving Temporal Variations in Data-Driven Flow Models Constructed by Motion Tomography ⋆

Dongsik Chang * **Fumin Zhang** *

* *Georgia Institute of Technology, Atlanta, GA 30308 USA (e-mail: {dsfrancis3,fumin}@gatech.edu).*

Abstract: Modeling and predicting ocean flow are great challenges in physical oceanography. To answer such challenges, mobile sensing platforms have been an effective tool for providing Lagrangian flow information. Such information is typically incorporated into ocean models using Lagrangian data assimilation which requires significant amount of computing power and time. Motion tomography (MT) constructs generic environmental models (GEMs) that combine computational ocean models with real-time data collected from mobile platforms to provide high-resolution predictions near the mobile platforms. MT employs Lagrangian data from mobile platforms to create a spatial map of flow in the region traversed by the mobile platforms. This paper extends the MT method to resolve the coupling between temporal variations and spatial variations in flow modeling. Along with Lagrangian data from a mobile sensor, Eulerian data are collected from a stationary sensor deployed in the region where the mobile sensor collects data. Assimilation of these two data sets into GEMs introduces a nonlinear filtering problem. This paper presents the formulation of such nonlinear filtering problem and derives a filtering method for estimating flow model parameters. We analyze observability for the derived filters and demonstrate that the resulting method improves navigation accuracy for mobile platforms.

Keywords: Motion tomography, data assimilation, nonlinear filtering.

1. INTRODUCTION

Ocean flow modeling is an active research area in oceanography. The geophysical dynamics of ocean flow can be modeled by partial differential equations (PDEs) that are solved numerically (e.g., Luettich et al., 1992; Bleck, 2002; Shchepetkin and McWilliams, 2005) under known initial and boundary conditions. However, the lack of direct measurements and the large scale of the ocean system hamper obtaining high spatio-temporal resolution solutions to these PDEs. In addition, because of uncertainties in ocean models, the accuracy of the solutions degrades in time. To overcome such challenges, the data collected from various ocean observing technologies can be used to estimate solutions. This technique is typically referred to as data assimilation (Apte et al., 2008).

Among various ocean observing technologies, earlier ones such as satellites and buoys provide Eulerian flow information. On the other hand, recent technologies such as mobile sensing platforms (e.g., autonomous underwater vehicles [AUVs]) are viewed as an effective tool for providing Lagrangian flow information (Curtin et al., 1993; Fratantoni and Haddock, 2009; Leonard et al., 2010). The introduction of mobile platforms triggered Lagrangian data assimilation scheme (Kuznetsov et al., 2003). This paper presents a computationally efficient method that fuses Lagrangian data collected by mobile sensing platforms along with Eulerian data into a high-resolution computational ocean model, which can also be used to navigate the vehicles.

The motions of mobile sensing platforms are affected by ambient flow; therefore, knowledge of the flow field can improve their navigation. Typical data assimilation methods (e.g., Kalman filtering and variational techniques such as three-dimensional/four-dimensional variational data assimilation [3DVAR/4DVAR]) for numerical ocean models require significant amount of computing power apart from that for supporting AUV navigation. In addition, existing regional ocean models are mostly formulated on a spatial resolution of a few kilometers, but AUV navigation requires sub-kilometer spatial resolutions.

To serve the need for high-resolution flow data, we develop generic environmental models (GEMs) (Chang et al., 2014, 2015, 2016) which are data-driven computational models combined with real-time data streams collected from AUVs. GEMs provide high-resolution predictions of ocean flow near the mobile platforms. For example, the ocean model proposed in Chang et al. (2014) approximates ocean flow using spatial and temporal basis functions. The model parameters are initialized based on historic data such as HF-radar observations or general oceanic circulation model output. Once initialized, the model assimilates Lagrangian flow estimates from a fleet of AUVs using a Kalman filter to update model parameters in real time.

This paper extends the motion tomography (MT) method (Wu et al., 2013; Chang et al., 2016) and continues the line of work to develop a data assimilation method for GEMs

⋆ The research work is supported by ONR grants N00014-10-10712 (YIP) and N00014-14-1-0635; and NSF grants OCE-1032285, IIS-1319874, and CMMI-1436284.

10.1016/j.ifacol.2016.10.160

using both Lagrangian and Eulerian data. The original MT method employs Lagrangian data collected from multiple AUVs to formulate an "inverse problem" that has been the core problem underlying medical CT (computerized tomography). By solving this inverse problem, MT constructs a high-resolution spatial map of flow in the region traversed by AUVs. In addition to the Lagrangian data collected by the AUVs, this paper also considers Eulerian data provided by stationary sensors such as a moored buoy. GEMs assimilate these two types of data streams by solving a nonlinear filtering problem. The fusion of the two data streams complement each other in that the Lagrangian data has much slower time scale than the Eulerian data but it provides necessary spatial coverage and spatial resolution for the GEM. We demonstrate that the resulting GEM improves navigation accuracy for AUVs.

The rest of the paper is organized as follows. Section 2 introduces a data-driven flow model and data sources that can be used for the model. Section 3 presents our data assimilation approach that combines Eulerian and Lagrangian data through a Kalman filter. Then, observability analysis for the designed Kalman filter is presented in Section 4. Section 5 demonstrates the proposed method through simulations and Section 6 concludes the paper.

2. FLOW FIELD MODELING

For fast computation and high resolution, data-driven flow models approximates ocean flow by using basis functions such as Fourier series, wavelets, piecewise polynomials, and splines. The weights of these basis functions are estimated from data streams collected from various sources.

2.1 Parametric Flow Field Model

Let us denote the time by $t \in \mathbb{R}$ and the position by $\mathbf{r} \in \mathbb{R}^2$. To approximate the temporal and spatial variations of flow, we use temporal and spatial basis functions. For position $\mathbf{r}$, we define spatial basis functions indexed by m as $\phi_m(\mathbf{r}) \in \mathbb{R}$. For time t, temporal basis functions indexed by n is given by $\psi_n(t) \in \mathbb{R}$. Then, with M spatial basis functions and N temporal basis functions, the x and y components of flow velocity $\mathbf{f}$ are represented by

$$\begin{aligned} f_x(\mathbf{r},t) &= \left(\sum_{m=1}^{M} \eta_{x,m}\phi_m(\mathbf{r})\right)\left(\sum_{n=1}^{N} \rho_{x,n}\psi_n(t)\right) \\ f_y(\mathbf{r},t) &= \left(\sum_{m=1}^{M} \eta_{y,m}\phi_m(\mathbf{r})\right)\left(\sum_{n=1}^{N} \rho_{y,n}\psi_n(t)\right), \end{aligned} \tag{1}$$

where η and ρ are constant parameters coupled with spatial and temporal basis functions, respectively.

Remark 1. Note that the model (1) is valid under the assumption of separation of variables. In other words, we assume that the flow field, as the solution of the geophysical PDEs, can be *approximated* by a space dependent term multiplied by a time dependent term. This assumption significantly simplifies filtering steps for our system later. A state equation for the parameters is formulated to account for the error associated with this approximation.

We define all the spatial parameters as $\eta_x = [\cdots, \eta_{x,m}, \cdots]^T$ and $\eta_y = [\cdots, \eta_{y,m}, \cdots]^T$ and all the temporal parameters as $\rho_x = [\cdots, \rho_{x,n}, \cdots]^T$ and $\rho_y = [\cdots, \rho_{y,n}, \cdots]^T$. By stacking them up, we define $\Theta_x = [\eta_x^T, \rho_x^T]^T$ and $\Theta_y = [\eta_y^T, \rho_y^T]^T$. Then, we can rewrite (1) as

$$\begin{aligned} f_x(\mathbf{r},t) &= h(\mathbf{r},t;\Theta_x) \\ f_y(\mathbf{r},t) &= h(\mathbf{r},t;\Theta_y), \end{aligned} \tag{2}$$

where $h(\mathbf{r},t;\cdot)$ is a nonlinear mapping from $\Theta_x, \Theta_y \in \mathbb{R}^{N+M}$ to $f_x, f_y \in \mathbb{R}$, respectively.

2.2 Data Sources of Flow Measurements

In this paper, we consider both Eulerian and Lagrangian data sources of flow measurements. Three of the typical data sources are reviewed.

The HF-radar system is a shore-based remote sensing system for coastal sea surface current observation using the over-the-horizon radar technology. Shore stations emit radio signals that bounce off surface waves and return to receiver. The received radio wave is used to compute ocean surface current movement relative to ocean surface wave movement. In general, hourly data with $6 \times 6\ km^2$ spatial resolution are published online with a three hour processing delay. In addition to this operational limit, even though HF-radar provides Eulerian data with a large spatial coverage, its spatial resolution is considered low for operation of mobile sensing platforms.

A buoy is a floating device that can be stationary at an installed location or mobile drifting with the ocean currents. In this paper, we only consider stationary buoys. Buoys with the current meter can measure ocean currents typically every hour at various depths from near the sea surface to near the sea bottom. Although a buoy provides Eulerian data on fast time scales, since it is fixed at one location, its flow data provides insufficient spatial variability for mobile sensing platforms.

In addition to the above Eulerian flow data sources, AUVs are important tools for providing Lagrangian flow data. AUVs typically have limited localization capabilities underwater (Zhang et al., 2015), so their actual positions are available when they are at the surface. Therefore, AUVs in general follow predicted trajectories generated prior to diving into the water. Since the motion of an AUV is perturbed by ambient flow, its actual trajectory deviates from its predicted trajectory. The difference of these two trajectories caused by deviation is referred to as the *motion-integration error*. Some AUVs estimate constant flow velocity along their last trajectories based on the motion-integration error. Both this flow estimate and the motion-integration error itself are very important data that provide Lagrangian flow information.

3. DATA ASSIMILATION

This section presents a data assimilation method to update the estimates of the parameters in (2) based on measurements from a buoy and trajectory information of an AUV. Given flow model (2), we use a state variable Θ to denote either Θ_x or Θ_y. Suppose a buoy provides Eulerian flow data with sampling period T_s. In addition, suppose an AUV navigates near the buoy, providing Lagrangian flow data every αT_s, $\alpha \in \mathbb{N}^+ \geq 2$ where $\mathbb{N}^+$ denotes positive integer. Since the time scale of buoy data is smaller, we let $\Theta_k = \Theta(kT_s)$ where k is the time step index.

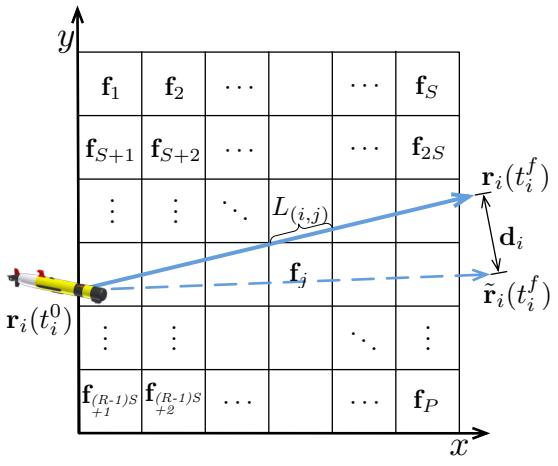

Fig. 1. Illustration of MT mapping formulation. Actual (the blue solid line) and predicted (the blue dashed line) vehicle trajectories are displayed.

To account for the inaccuracy of the ocean modeling techniques, we consider

$$\Theta_{k+1} = \Theta_k + w_k, \tag{3}$$

where w_k is the process noise at the kth step. We assume w_k is Gaussian with zero mean and known covariance Q_k.

For time step k and position $\mathbf{r}$, let us define an observation variable $z_k(\mathbf{r})$ to be observation of either $f_x(\mathbf{r}, kT_s)$ or $f_y(\mathbf{r}, kT_s)$. Provided that a buoy is deployed at $\mathbf{r}^E$, Eulerian flow observation at time step k is denoted by $z_k^E(\mathbf{r}^E)$. We use MT to convert the Lagrangian data collected from an AUV to a spatial map of flow. Figure 1 illustrates how MT mapping is formulated. (MT will be introduced in Section 3.1.) Suppose the map of the flow field contains P grid cells. Let $\mathbf{r}_j^L$ be a position that represents the jth grid cell. Then, we denote flow observation based on the Lagrangian data at time step k by $z_k^L(\mathbf{r}_j^L)$, $j = \{1, \cdots, P\}$.

For both Eulerian and Lagrangian observations defined as $z_k = [z_k^E(\mathbf{r}^E), z_k^L(\mathbf{r}_1^L), \cdots, z_k^L(\mathbf{r}_P^L)]$, the observation equation at time step k is given by

$$z_k = H_k(\Theta_k) + v_k, \tag{4}$$

where observation noise v_k is Gaussian with zero mean and known covariance matrix R_k and matrix H is defined as

$$H_k(\Theta_k) = \begin{bmatrix} h_k(\mathbf{r}^E, \Theta_k) \\ h_k(\mathbf{r}_1^L, \Theta_k) \\ \vdots \\ h_k(\mathbf{r}_P^L, \Theta_k) \end{bmatrix}, \tag{5}$$

where $h_k(\mathbf{r}, \Theta) = h(\mathbf{r}, kT_s; \Theta)$ defined in (2).

Even though state equation (3) is linear, we have nonlinear observation equation (4), leading to a nonlinear filtering problem for parameter estimation. To solve this nonlinear filtering problem, we decouple spatial and temporal parameter estimation and decompose a nonlinear filter into two linear sub-filters. Then, we consider one set of parameters as constant and solve the filtering problem for the other set of parameters. Since Lagrangian data through MT provide higher spatial variations than Eulerian data, we use Lagrangian data to update spatial parameters and Eulerian data to update temporal parameters.

3.1 Motion Tomography

MT estimates a flow field map from the motion-integration error and trajectory information of the AUV. Suppose an AUV travels in domain $\mathcal{D}$ (see Fig. 1) over observation interval $\mathcal{T} = [t^0, t^f]$ with no prior flow information and its position is available only at time t^0 and t^f. Let us define $\gamma(t), t \in \mathcal{T}$ as the vehicle trajectory. Then, the motion-integration error over $\mathcal{T}$ is given by

$$\mathbf{d}(\gamma, \mathcal{T}) = \int_{t^0}^{t^f} \dot{\mathbf{r}}(\tau, \mathbf{f}) - \dot{\tilde{\mathbf{r}}}(\tau, \tilde{\mathbf{f}}) d\tau = \int_{t^0}^{t^f} \mathbf{f}(\mathbf{r}, t) d\tau, \tag{6}$$

where $\mathbf{f}(\mathbf{r}, t)$ is real flow and prior flow information $\tilde{\mathbf{f}}$ is assumed zero.

After assuming time-invariant flow and substituting arc-length parameter ℓ for curve γ, given by

$$d\ell = s_{\text{tr}}(\mathbf{f}(\mathbf{r}))dt, \tag{7}$$

in which s_{tr} is the speed of the vehicle along its actual trajectory, we derive

$$\mathbf{d} = \int_\gamma \frac{1}{s_{\text{tr}}(\mathbf{f}(\mathbf{r}))} \mathbf{f}(\mathbf{r}) d\ell. \tag{8}$$

We discretize domain $\mathcal{D}$ into $P = R \times S$ grid cells with $D_{(r,s)}$ referring to the (r,s)th cell and define index $j = (r-1)S+s$ such that $D_j \equiv D_{(r,s)}$, $j = \{1, \cdots, P\}$. For the jth cell, let us denote flow velocity by $\mathbf{f}_j$ and assume a linear trajectory. From $\mathbf{r}(t^0)$, a vehicle trajectory within a cell depends on flow along the trajectory up to the current cell. Therefore, for trajectory γ of a vehicle traveling from $t = t^0$ to $t = t_j^f$, in which t_j^f is the time that the vehicle leaves cell D_j, we define a set of indices for cells the vehicle trajectory visits as $\kappa_j = \{n | [D_n] \cap \{\gamma(t)\}_{t \in [t^0, t_j^f]} \neq \emptyset\}$ and the length of a vehicle trajectory within D_j as $L_j(\mathbf{f}_{\kappa_j})$.

Based on the above discretization, (8) can be rewritten as

$$\mathbf{d} = \sum_{j=1}^{P} \frac{L_j(\mathbf{f}_{\kappa_j})}{s_{\text{tr}}(\mathbf{f}_j)} \mathbf{f}_j. \tag{9}$$

Separating the x and y components of flow, we have

$$d_x = \sum_{j=1}^{P} \frac{L_j(\mathbf{f}_{\kappa_j})}{s_{\text{tr}}^j(\mathbf{f}_j)} f_{x,j}, \qquad d_y = \sum_{j=1}^{P} \frac{L_j(\mathbf{f}_{\kappa_j})}{s_{\text{tr}}^j(\mathbf{f}_j)} f_{y,j}. \tag{10}$$

Defining $\mathbf{f}_x = [f_{x,1}, \cdots, f_{x,P}]^T$, $\mathbf{f}_y = [f_{y,1}, \cdots, f_{y,P}]^T$, and

$$\mathbf{L}(\mathbf{f}) = \begin{bmatrix} \frac{L_1(\mathbf{f}_{\kappa_1})}{s_{\text{tr}}^1(\mathbf{f}_1)} & \cdots & \frac{L_P(\mathbf{f}_{\kappa_P})}{s_{\text{tr}}^P(\mathbf{f}_P)} \end{bmatrix}, \tag{11}$$

we can rewrite (10) as

$$d_x = \mathbf{L}(\mathbf{f})\mathbf{f}_x, \qquad d_y = \mathbf{L}(\mathbf{f})\mathbf{f}_y, \tag{12}$$

where $\mathbf{f} = [\mathbf{f}_x^T, \mathbf{f}_y^T]^T$. The MT method creates a map of the underlying flow field $\mathbf{f}$ by solving the motion-integration error equations in (12) through an iterative process that consists of trajectory tracing and flow field estimation (Wu et al., 2013; Chang et al., 2016).

3.2 Spatial Parameter Estimation

Suppose the basis functions and the previous estimates of parameters for (1) are known. Let us omit subscripts x and y for simplicity of presentation. Given an estimated flow field map computed through MT, we fix all the temporal

parameters ρ using the previous estimates, $\hat{\rho}$, and estimate spatial parameters η. Then, in state vector Θ, η is the only unknown. Let us define $\Phi(\mathbf{r}) = [\cdots, \phi_m(\mathbf{r}), \cdots]^T$, $m = \{1, \cdots, M\}$ and $\Psi(t) = [\cdots, \psi_n(t), \cdots]^T$, $n = \{1, \cdots, N\}$. Then, flow velocity can be expressed as

$$f(\mathbf{r}, t) = \hat{\rho}^T \Psi(t) \Phi(\mathbf{r})^T \eta \tag{13}$$

which is linear in η. Suppose previous estimates of ρ are computed at time step $k-1$. Then, the state and observation equations for spatial parameter estimation are

$$\eta_{k+1} = \eta_k + w_k^\eta \tag{14}$$
$$z_k = H_k^\eta \eta_k + \nu_k^\eta, \tag{15}$$

where w_k^η is the process noise at the kth step, which is Gaussian with zero mean and known covariance Q_k^η and

$$H_k^\eta = \begin{bmatrix} \rho_{k-1}^T \Psi_k \Phi(\mathbf{r}_1^L)^T \\ \vdots \\ \rho_{k-1}^T \Psi_k \Phi(\mathbf{r}_P^L)^T \end{bmatrix}. \tag{16}$$

Then, the filtering equations are given by

$$\begin{aligned} \hat{\eta}_k^- &= \hat{\eta}_{k-1}^+ \\ P_k^{\eta-} &= P_{k-1}^{\eta+} + Q_{k-1}^\eta \\ K_k &= P_k^{\eta-} (H_k^\eta)^T (H_k^\eta P_k^{\eta-} (H_k^\eta)^T + R_k^\eta)^{-1} \\ \hat{\eta}_k^+ &= \hat{\eta}_k^- + K_k (\mathbf{z}_k - H_k^\eta \hat{\eta}_k^-) \\ P_k^{\eta+} &= (I - K_k H_k^\eta) P_k^{\eta-} (I - K_k H_k^\eta)^T + K_k R_k^\eta K_k^T, \end{aligned}$$

where $\hat{\eta}_k$ is the optimal estimate of η_k.

3.3 Temporal Parameter Estimation

We use Eulerian data to update temporal parameters. In contrast to the spatial parameter estimation, when Eulerian data are available, we fix all the spatial parameters η using the previous estimates, $\hat{\eta}$. Suppose Eulerian data are available at time step k and previous estimates of η were computed at $\lfloor k/\alpha \rfloor \alpha$. For temporal parameter estimation, the state and observation equations are given by

$$\rho_{k+1} = \rho_k + w_k^\rho \tag{17}$$
$$z_k = H_k^\rho \rho_k + \nu_k^\rho, \tag{18}$$

where w_k^ρ is the process noise for ρ at the kth step, which is Gaussian with zero mean and known covariance Q_k^ρ and

$$H_k^\rho = \eta_{\lfloor k/\alpha \rfloor \alpha}^T \Phi(\mathbf{r}^E) \Psi_k^T. \tag{19}$$

For temporal parameter estimation, the filtering equations are given by

$$\begin{aligned} \hat{\rho}_k^- &= \hat{\rho}_{k-1}^+ \\ P_k^{\rho-} &= P_{k-1}^{\rho+} + Q_{k-1}^\rho \\ K_k &= P_k^{\rho-} (H_k^\rho)^T (H_k^\rho P_k^{\rho-} (H_k^\rho)^T + R_k^\rho)^{-1} \\ \hat{\rho}_k^+ &= \hat{\rho}_k^- + K_k (\mathbf{z}_k - H_k^\rho \hat{\rho}_k^-) \\ P_k^{\rho+} &= (I - K_k H_k^\rho) P_k^{\rho-} (I - K_k H_k^\rho)^T + K_k R_k^\rho K_k^T, \end{aligned}$$

where $\hat{\rho}_k$ is the optimal estimate of ρ_k.

4. OBSERVABILITY ANALYSIS

Given a system with no control input, a Kalman filter converges if the system is uniformly completely observable (Jazwinski, 1970). We redefine uniform complete observability in Jazwinski (1970).

Definition 1. The linear system

$$\Theta_{k+1} = \Theta_k + w_k \tag{20}$$
$$z_k = H_k \Theta_k + \nu_k \tag{21}$$

is uniformly completely observable if there exist $\tau, \beta_1, \beta_2 > 0$ such that the observability Gramian $\mathcal{J}(k, k-\tau) = \sum_{j=k-\tau}^{k} H_j^T R_j^{-1} H_j$ satisfies $\beta_1 I \preccurlyeq \mathcal{J}(k, k-\tau) \preccurlyeq \beta_2 I$ for all $k > \tau$ where the dimension of I is defined accordingly. Here, R_j is the covariance matrix for noise ν_j.

Lemma 1. *For n linearly independent nonzero vectors $\mathbf{u}_i \in \mathbb{R}^n$, $\mathcal{M} = \sum_{i=1}^n \mathbf{u}_i \mathbf{u}_i^T \in \mathbb{R}^{n \times n}$ has full rank.*

Proof. Consider nonzero vector $\mathbf{v}_1 \in \text{span}\{\mathbf{u}_2, \cdots, \mathbf{u}_n\}^\perp$. Then, $\mathcal{M}\mathbf{v}_1 = (\mathbf{u}_1 \mathbf{u}_1^T)\mathbf{v}_1 = \mathbf{u}_1(\mathbf{u}_1^T \mathbf{v}_1)$ is a nonzero scalar multiple of $\mathbf{u}_1$. Similarly, for $\mathbf{v}_i \in \text{span}\{\mathbf{u}_j\}_{j \neq i}^\perp$, $\mathcal{M}\mathbf{v}_i$ is a nonzero scalar multiple of $\mathbf{u}_i$. In other words, nonzero scalar multiples of each $\mathbf{u}_i$ are in the range of $\mathcal{M}$ and the dimension of the range of $\mathcal{M}$ is n, which is equivalent to $\mathcal{M}$ having full rank (c.f. Horn and Johnson, 1985, pg. 13). □

In the following theorem, we prove uniform complete observability for spatial parameter estimation:

Theorem 1. *The system (14)–(15) is uniformly completely observable if the following conditions are met:*

(Cd1) *The matrix R_j^η is uniformly bounded for all j (i.e., $\beta_3 I_{(P+1)\times(P+1)} \preccurlyeq R_j^\eta \preccurlyeq \beta_4 I_{(P+1)\times(P+1)}$ for some constants $\beta_3, \beta_4 > 0$.*

(Cd2) *Among $\Phi(\cdot)$'s evaluated at the position of the buoy, $\mathbf{r}^E$, and the positions of the grid cells, $\mathbf{r}_i^L$, $i = \{1, \cdots, P\}$, at least M $\Phi(\cdot)$'s are linearly independent.*

Remark 2. Condition (Cd2) can be satisfied by choosing spatial basis functions appropriately. Consider Gaussian radial basis functions (GRBFs) indexed by m, $\phi_m(\mathbf{r}) = \exp\left(-\frac{\|\mathbf{r}-\mathbf{c}_m\|}{2\sigma^2}\right)$, where $\mathbf{c}_m$ is the center and σ is the width. If we use GRBFs as spatial basis functions for $\Phi(\mathbf{r}) = [\cdots, \phi_m(\mathbf{r}), \cdots]^T$, $m = \{1, \cdots, M\}$, (Cd2) can be satisfied by choosing M different centers.

Proof. For system (14)–(15), we have observability Gramian $\mathcal{J}_\eta(k, k-\tau) = \sum_{j=k-\tau}^{k} (H_j^\eta)^T (R_j^\eta)^{-1} H_j^\eta$. From (Cd1), R_j^η is positive definite and bounded above and below. Therefore, we obtain $\beta_4^{-1} \sum_{j=k-\tau}^{k} (H_j^\eta)^T H_j^\eta \preccurlyeq \mathcal{J}_\eta(k, k-\tau) \preccurlyeq \beta_3^{-1} \sum_{j=k-\tau}^{k} (H_j^\eta)^T H_j^\eta$ for all $k > \tau$. Next, we prove that $\sum_{j=k-\tau}^{k} (H_j^\eta)^T H_j^\eta$ is positive definite. We can compute

$$\begin{aligned} (H_j^\eta)^T H_j^\eta &= \begin{bmatrix} \rho_{j-1}^T \Psi_j \Phi(\mathbf{r}_1^L)^T \\ \vdots \\ \rho_{j-1}^T \Psi_j \Phi(\mathbf{r}_P^L)^T \end{bmatrix}^T \begin{bmatrix} \rho_{j-1}^T \Psi_j \Phi(\mathbf{r}_1^L)^T \\ \vdots \\ \rho_{j-1}^T \Psi_j \Phi(\mathbf{r}_P^L)^T \end{bmatrix} \\ &= \left(\rho_{j-1}^T \Psi_j \Phi(\mathbf{r}_1^L)^T\right)^T \rho_{j-1}^T \Psi_j \Phi(\mathbf{r}_1^L)^T + \cdots \\ &\quad + \left(\rho_{j-1}^T \Psi_j \Phi(\mathbf{r}_P^L)^T\right)^T \rho_{j-1}^T \Psi_j \Phi(\mathbf{r}_P^L)^T \\ &= \left(\rho_{j-1}^T \Psi_j\right)^2 \left[\Phi(\mathbf{r}_1^L)\Phi(\mathbf{r}_1^L)^T + \cdots + \Phi(\mathbf{r}_P^L)\Phi(\mathbf{r}_P^L)^T\right]. \end{aligned}$$

The quadratic scalar term $\left(\rho_{j-1}^T \Psi_j\right)^2$ is always positive unless the temporal component of flow is zero everywhere. Let us define $\mathcal{M}^\eta = [\Phi(\mathbf{r}_1^L)\Phi(\mathbf{r}_1^L)^T + \cdots + \Phi(\mathbf{r}_P^L)\Phi(\mathbf{r}_P^L)^T]$. All the terms inside the bracket are rank-one positive-semidefinite matrices. From (Cd2) and Lemma 1, $\mathcal{M}^\eta$ has full rank and is positive definite. Therefore, $\beta_5 I_{M\times M} \preccurlyeq \mathcal{M}^\eta \preccurlyeq \beta_6 I_{M\times M}$ for some constants $\beta_5, \beta_6 > 0$. □

Remark 3. Suppose multiple AUVs collect Lagrangian data. Regardless of the number of AUVs, the number of grid cells does not change, preserving the dimension of observation matrix H^η. Instead, using multiple AUVs will increase the rate of visiting all the grid cells and the chance of generating linearly independent $\Phi(\cdot)$'s. Therefore, the uniform complete observability condition can be satisfied in shorter time window than using just a single AUV.

In the following theorem, we prove uniform complete observability for temporal parameter estimation:

Theorem 2. *System* (17)–(18) *is uniformly completely observable if* (Cd1) *and the following condition are met:* (Cd3) *The sampling period T_s is chosen such that at least N Ψ_j's, $j \in [k-\tau, k] \subset \mathbb{N}^+$ are linearly independent.*

Proof. For system (17)–(18), we have observability Gramian $\mathcal{J}_\rho(k, k-\tau) = \sum_{j=k-\tau}^{k} (H_j^\rho)^T (R_j^\rho)^{-1} H_j^\rho$. From (Cd1), R_j^ρ is positive definite and bounded above and below. Therefore, we obtain $\beta_4^{-1} \sum_{j=k-\tau}^{k} (H_j^\rho)^T H_j^\rho \preccurlyeq \mathcal{J}_\rho(k, k-\tau) \preccurlyeq \beta_3^{-1} \sum_{j=k-\tau}^{k} (H_j^\rho)^T H_j^\rho$ for all $k > \tau$. Next, we prove that $\sum_{j=k-\tau}^{k} (H_j^\rho)^T H_j^\rho$ is positive definite. We can compute

$$
\begin{aligned}
(H_j^\rho)^T H_j^\rho &= \left[\eta_{\lfloor j/\alpha \rfloor \alpha}^T \Phi(\mathbf{r}^E) \Psi_j^T \right]^T \left[\eta_{\lfloor j/\alpha \rfloor \alpha}^T \Phi(\mathbf{r}^E) \Psi_j^T \right] \\
&= \left(\Phi(\mathbf{r}^E)^T \eta_{\lfloor j/\alpha \rfloor \alpha} \eta_{\lfloor j/\alpha \rfloor \alpha}^T \Phi(\mathbf{r}^E) \right) \Psi_j \Psi_j^T
\end{aligned}
$$

The quadratic term in the parenthesis is always positive unless the spatial component of flow is zero everywhere. Let $\mathcal{M}^\rho = \sum_{j=k-\tau}^{k} \Psi_j^T \Psi_j$. From (Cd3) and Lemma 1, $\mathcal{M}^\rho$ has full rank and is positive definite. Therefore, $\beta_7 I_{N\times N} \preccurlyeq \mathcal{M}^\rho \preccurlyeq \beta_8 I_{N\times N}$ for some constants $\beta_7, \beta_8 > 0$. □

Remark 4. The increased number of buoys will increase the dimension of the observation matrix H^ρ. With multiple buoys, by choosing locations of buoys such that the rank of the observation matrix increases, the uniform complete observability condition can be satisfied over a shorter time window than using just a single buoy.

5. SIMULATION RESULTS

To show that the proposed method resolves temporal variations for MT, we compare two implementations of GEMs: GEM-EL assimilating both Eulerian and Lagrangian data and GEM-L assimilating Lagrangian data only. We use a data-driven computational model in (1) as a GEM. For spatial basis functions, we use GRBFs. For temporal basis functions, we decompose ocean flow into tidal and non-tidal components. Then, we use a series of sinusoidal basis functions as temporal basis functions for tidal flow and weighted Laguerre polynomials as those for non-tidal flow.

Flow model (1) is initialized by using a month-long set of post-processed historic HF-radar data with 3×3 km^2 spatial resolution and one hour temporal resolution. In our simulation, one hour corresponds to one time step. For the HF-radar data, $N = 3$ major constituents are used to generate temporal basis functions for the tidal component. For the non-tidal component, we use 0th to 4th order ($L = 5$) Laguerre polynomials as temporal basis functions. To account for spatial variations, $M = 5$ GRBFs are used. After the model initialization, we select a segment of HF-radar data over the period followed by that of the initialization data to simulate the "true" flow field, which is constructed by real sea surface flow observation data from November 9, 2011 11:53pm. A buoy is deployed at location $(0, 0)$ in the domain of the simulated field. Figure 2 shows time-series flow measured by the buoy.

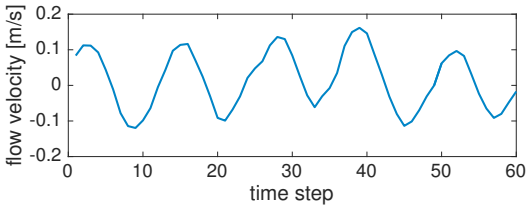

(a) x component of flow.

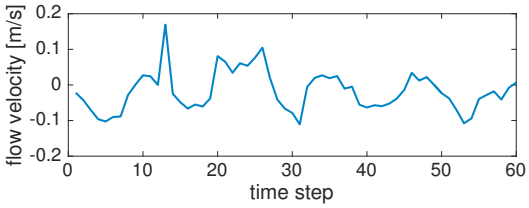

(b) y component of flow.

Fig. 2. Time-series Eulerian flow data for 60 time steps.

For estimation of the flow model parameters, we randomly generate initial parameters from the uniform distribution on $[-0.5, 0.5]$. We assume buoy data are available every time step. Around the buoy, an AUV travels across the buoy every time step, criss-crossing the domain. Since the most dominant tidal constituent for the simulated flow field has a period of 12.42 hours, to reduce the influence of temporal variations of flow from the mapping results, we create a $P = 6 \times 6$ grid map of flow through MT every $\alpha = 12$ time steps. Then, we update parameters using the proposed method with $Q_k^\rho = 10^{-2} I_{(L+2N+2)\times(L+2N+2)}$, $Q_k^\eta = 10^{-2} I_{M\times M}$, $R_k^\rho = 10^{-4} I_1$, and $R_k^\eta = 10^{-4} I_P$.

We compute the error between the simulated "true" flow fields and the estimated flow fields. Then, spatial mean of the square root of the errors are computed (see Fig. 3). Since Lagrangian data are assimilated after the first 12 time steps, we compute errors from $k = 12$. Since GEM-EL incorporates both spatial and temporal variations of flow, overall it shows lower values and smaller variance of the errors than GEM-L. Temporally averaged errors are displayed in the figures. Over the period, the results show that GEM-EL has 10 percent lower error and validates that our method resolves temporal variations for MT.

To demonstrate the effectiveness of the proposed method, we simulate two virtual mooring vehicles: one guided by GEM-EL and the other by GEM-L. Both vehicles are deployed at $(0, 0)$, and after time step $k = 12$, they start attempting to cancel the flow using flow estimates by either GEM-EL or GEM-L until $k = 60$. Here, we assume that perfect flow cancellation is possible. Figure 4 shows the trajectories of both vehicles. The vehicle guided by GEM-EL (the blue line) successfully stays within a region close to the origin. However, with no knowledge of temporal variation of flow, the vehicle guided by GEM-L

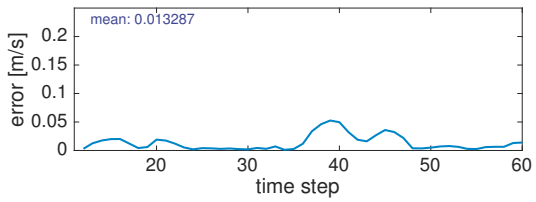

(a) GEM-EL.

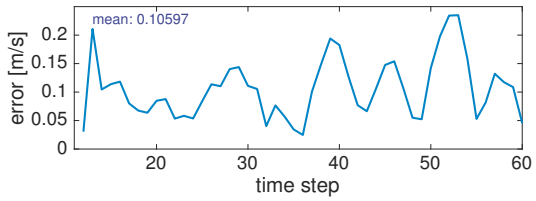

(b) GEM-L.

Fig. 3. Spatial mean square error.

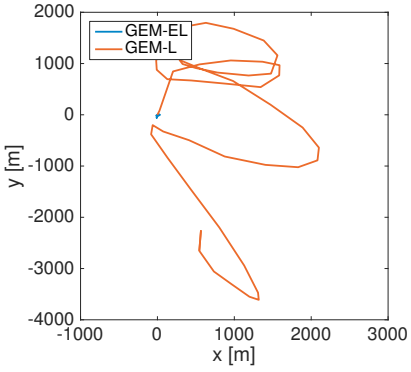

Fig. 4. Virtual mooring vehicles.

(the orange line) fails to stay close to the origin. These results show that the resulting GEM can improve the navigation accuracy for AUVs.

6. CONCLUSION AND FUTURE WORK

This paper presents a method for assimilating both Lagrangian and Eulerian data into a data-driven computational flow model constructed as a generic environmental model (GEM). In the proposed method, Lagrangian data are processed through our motion tomography method to create a spatial map of flow. Due to the coupling between temporal and spatial components in the flow model, temporal and spatial parameter estimation for the GEM falls into a nonlinear filtering problem. By solving this nonlinear filtering problem using two linear sub-filters, our method estimates temporal parameters using Eulerian data and spatial parameters using Lagrangian data. Assimilation of both data streams improves a GEM by resolving temporal variability for MT and the resulting GEM increases the navigation performance of AUVs.

ACKNOWLEDGEMENTS

We would like to thank Catherine R. Edwards and Dana Savidge at the Skidaway Institute of Oceanography for providing us with HF-radar data.

REFERENCES

Apte, A., Jones, C.K.R.T., Stuart, A.M., and Voss, J. (2008). Data assimilation: Mathematical and statistical perspectives. *International Journal for Numerical Methods in Fluids*, 56(8), 1033–1046.

Bleck, R. (2002). An oceanic general circulation model framed in hybrid isopycnic-Cartesian coordinates. *Ocean Modelling*, 37, 55–88.

Chang, D., Liang, X., Wu, W., Edwards, C.R., and Zhang, F. (2014). Real-time modeling of ocean currents for navigating underwater glider sensing networks. In A. Koubâa and A. Khelil (eds.), *Cooperative Robots and Sensor Networks*, volume 507 of *Studies in Computational Intelligence*, 61–75. Springer Berlin Heidelberg.

Chang, D., Wu, W., and Zhang, F. (2016). Glider CT: Analysis and experimental validation. In N.Y. Chong and Y.J. Cho (eds.), *Distributed Autonomous Robotic Systems*, volume 112 of *Springer Tracts in Advanced Robotics*, 285–298. Springer Japan.

Chang, D., Zhang, F., and Edwards, C.R. (2015). Real-time guidance of underwater gliders assisted by predictive ocean models. *Journal of Atmospheric and Oceanic Technology*, 32(3), 562–578.

Curtin, T.B., Bellingham, J.G., Catipovic, J., and Webb, D. (1993). Autonomous oceanographic sampling networks. *Oceanography*, 6(3), 86–94.

Fratantoni, D.M. and Haddock, S.H. (2009). Introduction to the autonomous ocean sampling network (AOSN-II) program. *Deep Sea Research Part II: Topical Studies in Oceanography*, 56(3-5), 61.

Horn, R.A. and Johnson, C.R. (1985). *Matrix Analysis*. Cambridge University Press.

Jazwinski, A.H. (1970). *Stochastic processes and filtering theory*. Dover Publications.

Kuznetsov, L., Ide, K., and Jones, C.K.R.T. (2003). A method for assimilation of Lagrangian data. *Monthly Weather Review*, 131(10), 2247–2260.

Leonard, N.E., Paley, D.A., Davis, R.E., Fratantoni, D.M., Lekien, F., and Zhang, F. (2010). Coordinated control of an underwater glider fleet in an adaptive ocean sampling field experiment in Monterey Bay. *Journal of Field Robotics*, 27(6), 718–740.

Luettich, R.A., Westerink, J.J., and Scheffner, N.W. (1992). ADCIRC: An advanced three-dimensional circulation model for shelves, coasts, and estuaries. Report 1. Theory and methodology of ADCIRC-2DDI and ADCIRC-3DL. Technical report, Coastal Engineering Research Center, Vicksburg, Mississippi (U.S.).

Shchepetkin, A.F. and McWilliams, J.C. (2005). The regional oceanic modeling system (ROMS): A split-explicit, free-surface, topography-following-coordinate oceanic model. *Ocean Modelling*, 9(4), 347–404.

Wu, W., Chang, D., and Zhang, F. (2013). Glider CT: Reconstructing flow fields from predicted motion of underwater gliders. In *Proceedings of the Eighth ACM International Conference on Underwater Networks and Systems*, 47.

Zhang, F., Marani, G., Smith, R.N., and Choi, H.T. (2015). Future Trends in Marine Robotics [TC Spotlight]. *IEEE Robotics and Automation Magazine*, 22(1), 14–122.